Kobe University Repository : Kernel

PDF issue: 2025-12-04

Intermediate band electron wave function localization effect on the efficiency limits of InAs/GaAs quantum dot solar cell

Mehdipour, Amir
Ogawa, Matsuto
Souma, Satofumi

(Citation)
Memoirs of the Graduate Schools of Engineering and System Informatics Kobe University,6:18-24

(Issue Date)
2014

(Resource Type)
departmental bulletin paper

(Version)
Version of Record

(URL)
https://hdl.handle.net/20.500.14094/81008842

Memoirs of the Graduate Schools of Engineering and System Informatics Kobe University
No. 6, pp. 18–24, 2014. doi:10.5047/gseku.e.2014.003

Intermediate band electron wave function localization effect on the efficiency limits of InAs/GaAs quantum dot solar cell

Amir Mehdipour, Matsuto Ogawa, and Satofumi Souma

Department of Electrical and Electronic Engineering, Kobe University,
1-1 Rokkodai, Nada, Kobe 657-8501, Japan

(Received May 22, 2014; Accepted September 30, 2014; Online published November 21, 2014)

Keywords: Intermediate Band Solar Cell, Quantum Dots, Tight-Binding Method

In the conventional detailed balance theory of quantum dot intermediate band solar cell (QD-IBSC), the electron wave function is assumed to be completely delocalized. Such wavefunctions are known to reduce thermal losses and enhance the photon-harvesting efficiency of an intermediate band. The aim of this study is to investigate the accuracy of the assumption of such "metallic-like IB" in determining the efficiency of IBSC in the presence of one or two IBs. According to our calculations for cubic model QD structures based on the finite element method, the electronic wave functions are strongly concentrated in the QD regions for the realistic QD spacing. The influence of such electron localization effects on the cell efficiency is then carefully examined by introducing the effective electron filling factor along with the detailed balance theory, with particular attention given to the roles played by the number of IBs and sunlight concentration. While the electron localization in IBs is detrimental for cell efficiency, the use of IBs is demonstrated to be still beneficial and improve the efficiency significantly under full sunlight concentration.

1. Introduction

Luque and Marti showed that the introduction of an intermediate band (IB) in the band gap of a regular semiconductor enables the absorption of two "below the gap photons" via the IB in a two-step process. In other words, electrons can be excited from the valence band (VB) to the conduction band (CB) via the IBs in a multiple excitation process, as well as via the direct excitation path. For this mechanism, the detailed balance theory predicts that the maximum efficiency of the solar cell (SC) can be up to 63.1% for an IBSC with a single IB. This compares favorably with the Shockley–Queisser (SQ) efficiency limit of 40.7% under the maximum concentration of sunlight (46000 suns) for a single junction SC [1, 2, 3]. The IBSC can be achieved using materials that have intrinsic IBs between VB and CB [4, 5] or by forming the IB by quantum-dot superlattices (QDSLs) inside conventional semiconductors. The latter scheme is called the quantum dot intermediate band solar cells (QD-IBSCs) [6, 7, 8, 9, 10].

Generally, a QD-IBSC structure is fabricated by sandwiching the QDSLs inside the p-n junction, as shown in Fig. 1. One-dimensionally ordered QDSLs with closely spaced QDs in the z direction is believed to allow QD electron wave functions to overlap and form the desired IB or IBs. There have been several experimental reports of vertical one-dimensional structures [11, 12], as well as three-dimensional ones [13, 14, 15], followed by the recent successful fabrication of a QD-IBSC module [16, 17]. Further progress in self-assembly growth is expected to result in well-ordered QDSLs with closely spaced QDs to form better IBs. In this structure, inserting two layers of conventional semiconductors between the stack of QD layers and the electrodes is beneficial to sustain the flat-band potential in the QDSL region and maximize the effect of the QD layers (Fig. 1). Without the semiconductor layers, although the QDSL region is doped to make the IB half filled with electrons through modulation doping at the barrier region, IBs in some QD layers close to the p-type region become empty and to the n-type region become full. Thus, some QD layers do not contribute to the transitions through IBs without those additional layers [8].

The ideal IBSC with a single IB with completely delocalized electron wave function and infinitesimal bandwidth has been evaluated thus far by many researchers who suggest that a completely delocalized IB wave function is necessary to reduce thermal losses and to enhance the photon-harvesting efficiency of an intermediate band (IB) [18, 6, 19, 20, 21]. In reality, however, electron wave function is not completely delocalized but is rather localized inside QDs to some extent, with the extent of such localization varying for the different IBs in the case of multiple IBs. Moreover, understanding the impact of the sunlight concentration on the efficiency limit of QD-IBSC is of interest when the electron wave-function localization effect mentioned above is considered.

Motivated by these considerations, we perform a numerical study of the influence of electron wave-function localization on the efficiency limit of QD-IBSC, with a special focus on the roles played by the number of IBs and the sunlight concentration. While there have been several reports on ideal QD-IBSC with multiple IBs [22, 23, 24], in this study, we focus on the influence of non ideality in QD-IBSC caused by IB wave-function

localization. We study the dependence of the efficiency limits on the extent of the IB wave-functions for the case of concentrated and unconcentrated sunlight illuminations.
The paper is organized as follows. In the next section, we discuss the QD-IBSC structure models and their electronic properties. In Sec. III, we present the discussion of the detailed balance efficiency. In Sec. IV, we summarize our findings.

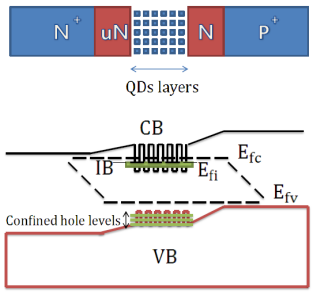

Figure 1: Simplified structure and band diagram of QD-IBSC with two field-damping layers.

2. Structure model and electronic properties

2.1. Structure models

In this study, we consider the QDSLs made of InAs QDs embedded in a GaAs barrier, which can be obtained experimentally by the self-assembly process. For the theoretical analysis of the efficiency in such InAs/GaAs based QD-IBSC, first, understanding the electronic energy eigenstates of electrons confined in such QDSLs by solving the three-dimensional effective-mass equations is necessary. Here, note that the actual self-assembled quantum dots are grown on the wetting layer (WL) that behaves like a quantum well with additional levels close to the CB minimum in the barrier material. As a consequence, the edge of the CB is lowered to the WL level [25], leading to the reduction of the bandgap in the barrier material from the original 1.43 eV GaAs value to ~ 1.3 eV at room temperature, as reported in Ref. [6]. We use this reduced bandgap concept in our model to estimate the efficiency limit. Then, neglecting the strain and using the valence band offset of 0.17 eV [26] and the InAs band gap of 0.36 eV, the CB offset (i.e., the QD potential height in the CB) is estimated to be 0.77 eV. While strain has been suggested to cause the reduction of the CB offset [27], in this study, we first neglect this effect because of our focus on qualitative understanding. We then comment on the effects of strain in our discussion of the numerical results.
Once the potential height is known, we can solve the CB effective mass equation (Schrödinger equation) for understanding the energy eigenstates of the electrons confined in the QD,

$$\mathcal{H}\Psi(\mathbf{r}) = E\Psi(\mathbf{r}), \tag{1}$$

$$\mathcal{H} = -\nabla\frac{\hbar^2}{2m^*(\mathbf{r})}\nabla + V(\mathbf{r}), \tag{2}$$

where $2\pi\hbar$ is the Planck's constant, and $m^*(\mathbf{r})$ and $V(\mathbf{r})$ are the effective mass and the QDSL confinement potential, respectively, given by $m^* = 0.024m_0$ and $V(\mathbf{r}) = 0$ inside the InAs QD, and by $m^* = 0.067m_0$ and $V(\mathbf{r}) = 0.77$ eV outside the QD (i.e., in the GaAs region), with m_0 being the free electron mass. While the methodology presented below is valid, independent of the details of the geometrical structure of each QD (i.e., closed boundary surface dividing the QD and barrier regions), in this study, we consider the cubically shaped QDs with length $L_{\rm QD} = 9$ nm for simplicity, aiming at obtaining two IBs. Although the shape of the experimentally obtained QD is similar to a trapezoidal or a pyramidal shape, even a simpler geometrical shape can capture the essence of the physics in QDSLs as reported in Refs. [27, 28]. This is especially true for this study, because our focus here is to qualitatively elucidate the effect of IB wave-function localization on the SC efficiency for the case of multiple IBs. Therefore, a study based on a simple QD shape is meaningful. The impact of the QD shape on the efficiency will be studied in detail in the future research.

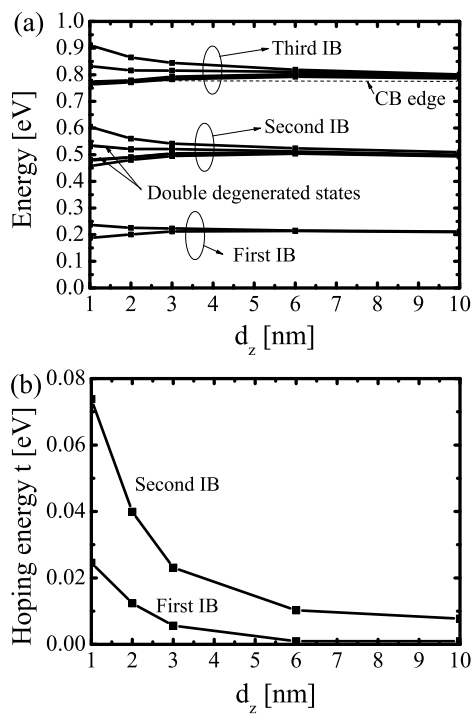

Figure 2: (a) Energy eigenvalues are plotted as a function of the inter-QD separation The third group of eigenstates will be formed above the CB edge. (b) Tight-binding hopping energies for the first and second IBs are plotted as a function of the inter-QD separation.

2.2. Study of two QDs

As the first step of our analysis, we consider a model consisting of two cubic InAs QDs with the inter-QD separation smaller than 10 nm surrounded by a GaAs region with the side lengths $L_z = 2 \times d_z + 2 \times L_{\rm QD}$ along the z (stacking) direction and $L_{x(y)} = L_{\rm QD} + d_{x(y)}$ along the transverse direction, where

$d_{x(y)}$ is the QD spacing in the $x(y)$ direction related to the transverse QD's density. In this study, we assume a relatively small value of $d_x = d_y = 5$ nm to capture the essential features in this system. We note that in this case, the electronic coupling between neighboring QDs in x and y directions can be safely ignored.

For such a model, Eq. (1) is solved using the finite element method (FEM) to obtain the energy eigenvalues and eigenvectors. In Fig. 2(a), the calculated energy eigenvalues are plotted as a function of the inter-QD spacing d_z. Here, we can observe three sets of eigenenergies, where the nth set (contributing to the nth IB) originates from the nth energy eigenvalue (without considering degeneracy) in the isolated QD, which splits into multiple levels with larger level splitting for a smaller QD spacing d_z. It is also apparent in this figure that the second IB consists of six energy levels, four of which resulted from the hopping between the two degenerate states in each QD.

Using the energy level splitting shown in Fig. 2(a), the effective hopping energy factor t can be evaluated in the framework of the tight-binding (TB) model as follows. We suppose that the mth eigenfunction of an isolated QD centered at $\mathbf{r}_i = (x_i, y_i, z_i)$ is written as $\phi_m(\mathbf{r} - \mathbf{r}_i)$, and its eigenenergy is ϵ_m. Then, because the transfer between two neighboring QD wave functions with different m can be ignored owing to either different symmetries of the wave functions or a large energy difference, the wave function in the system consisting of two QDs can also be specified by the same eigenvalue index m. The wave function is given approximately by a linear combination of the isolated QD wave functions as follows:

$$\Psi_m(\mathbf{r}) = \sum_{i=1}^{N} c_i \phi_m(\mathbf{r} - \mathbf{r}_i), \tag{3}$$

where $N = 2$ for the system consisting of two QDs, and the corresponding mth energy eigenvalue is E_m, which is, in general, different from ϵ_m. By substituting the above wave function into the CB effective mass equation, i.e., Eq. (1), we obtain E_m in the orthogonal TB approximation as follows:

$$E_m^{(\pm)} = \epsilon_m \pm t_m, \tag{4}$$

with $t_m = -\int d^3r \phi_m^*(\mathbf{r} - \mathbf{r}_2)\mathcal{H}\phi_m(\mathbf{r} - \mathbf{r}_1)$ interpreted as the hopping energy between the two QDs. This hopping energy can be related phenomenologically to the energy level splitting ΔE_m calculated using the FEM (in Fig. 2(a)) by $\Delta E_m = 2|t_m|$ in this two QD model. The obtained IB dependent hopping energy $|t_m|$ is plotted as a function of d_z in Fig. 2(b). Here, we note that the hopping energy factor evaluated using the maximum ΔE for each d_z is larger for the second IB is larger than for the first IB. This is because the wave function of the second IB can penetrate deeper into the barrier than that of the first IB; this gives rise to stronger hopping. Considering Fig. 2(a) and the potential height of 0.77 eV, the third IB is found to form slightly above the CB edge and consequently can be omitted from the list of IBs in the band gap of the material.

2.3. Stacked QDs layers

The calculated tight-binding (TB) hopping energies between two adjacent QDs for the first (t_{IB1}) and second (t_{IB2}) IBs [Fig. 2(b)] are the key parameters for understanding the formation of IBs for a stack of QD layers. To estimate the band width of IBs and the electron wave functions of a QDSL consisting of N QDs, we again use the TB approach described above. First, we substitute Eq. (3) into the CB effective mass equation, i.e., Eq. (1), where N is no longer necessarily equal to two but is rather equal to the number of QDs. We then obtain E_m in the orthogonal TB approximation as follows:

$$-t_m c_{i-1} + \epsilon_m c_i - t_m c_{i+1} = E_m c_i, \tag{5}$$

where E_m is the mth band energy, and $t_m \equiv -\int d^3r \phi_m^*(\mathbf{r} - \mathbf{r}_{i+1})\mathcal{H}\phi_m(\mathbf{r} - \mathbf{r}_i)$ is the hopping energy shown in Fig. 2(b), which is obtained phenomenologically based on the FEM calculations of the two QDs. If the number N of stacked QDs is sufficiently large for the system to be considered as periodic along the z (stacking) direction, the coefficients c_i can be obtained from $c_{i+1} = e^{ika}c_i$, where k and $a \equiv z_{i+1} - z_i$ are the wave number and lattice constant along the z direction, respectively. We then obtain $E_m(k)$ using the equation as follows:

$$E_m(k) = \epsilon_m - 2t_m \cos ka, \tag{6}$$

which results in IB width $\Delta E_m = 4|t_m|$.

We note that the band width of the second IB (i.e., $m \in$ 2nd IB) is always larger than that of the first IB (i.e., $m \in$ 1st IB) because of the larger wave function penetration into the barrier region of the second IB than that of the first IB. For example, when $d_z = 1$ nm and $N = 100$, the band widths are $\Delta E_{\mathrm{IB1}} \simeq 0.1$ eV and $\Delta E_{\mathrm{IB2}} \simeq 0.3$ eV. Such large values of the IB band width are unfavorable for the proper functioning of the device. In contrast, when $d_z = 10$ nm and $N = 100$, the IB band widths are limited to just a few meV ($\Delta E_{\mathrm{IB1}} \simeq 4$ meV, $\Delta E_{\mathrm{IB2}} \simeq 30$ meV), which are sufficiently small for the efficient functioning of the IBSC. On the basis of the hopping energy values presented in Fig. 2(b), we determined that the inter-QD spacing must be larger than 5 nm to ensure that the IB band widths remain below 50 meV.

In the next section, we discuss the detailed balance efficiency with the assumptions of the representative positions of the IBs estimated from Fig. 2(a) as follows. For the calculations with two IBs, E_{14} is taken from the reduced band gap of GaAs and is equal to 1.3 eV, E_{12} is estimated from the energy difference between the VB edge and the first IB and is equal to 0.7 eV, E_{23} is taken from the energy difference between the first and the second IBs and is equal to 0.32 eV, E_{34} is the energy difference between the second IB and the CB edge and is equal to 0.28 eV. For the calculations with one IB, $E_{13} = 1.3$ eV, $E_{12} = 0.7$ eV, and $E_{23} = 0.6$ eV. Here we have implicitly assumed a sufficiently large inter-QD spacing of d_z = 10 nm for the negligible IB band widths.

3. Detailed balance efficiency: influence of IB wavefunction localization

3.1. Theoretical framework of the detailed balance efficiency incorporating the electron filling factor (EFF)

Depending on the volumes and shapes of QDs, solar cells can be fabricated with either a single IB or multiple IBs. For both cases, the efficiency can be estimated using the detailed balance theory with the assumptions as follows: (i) only radiative recombination is possible, (ii) a single electron-hole pair is generated per photon, (iii) there is a constant quasi-Fermi level for each band, (iv) every photon is absorbed in the most favorable manner with the largest threshold energy, (v) carrier mobility is sufficiently high, and (vi) the solar cell has a large number of QD layers and is sufficiently thick to maximize the photon absorption. The number of photons per unit area radiated by a black body object, such as the sun or the solar cell, for the energy interval of E_l, E_h is given by

$$\dot{N}(E_l, E_h, T, \mu) = X \frac{2\pi}{h^3 c^2} \int_{E_l}^{E_h} \frac{E^2}{\exp\left(\frac{\epsilon-\mu}{k_{\mathrm{B}}T}\right) - 1} dE, \quad (7)$$

where E is the energy, μ is the chemical potential associated to the transition, T is the temperature, h is the Planck's constant, c is the speed of light, and k_{B} is the Boltzmann constant. X is the sun concentration ratio; in this study, we used $X = 1$ and 1/46000 for fully concentrated and unconcentrated sunlight, respectively.

The generation rate is proportional to the sun photon flux with $\mu = 0$ and the solar temperature $T_{\mathrm{s}} = 6000$ K assuming isotropic cell illumination [i.e., assumption (vi)]. The recombination rate is obtained with the semiconductor body temperature $T_{\mathrm{a}} = 300$ K and the chemical potential μ defined by the difference between two quasi-Fermi levels (QFLs) assigned for each band under consideration.

Before starting our derivation of the equations for the efficiency, we introduce a parameter to represent the wave function localization in the QD region. For a localized IB wave function, the relative volume in which the IB wave functions are nonzero is the representative of the IB light absorption; i.e., if the IB wave functions penetrate more into the barrier region, we can expect some extra photons to be absorbed by IBs. Therefore, such a parameter (EFF) can be defined as the ratio between the integrated probability density inside and outside QDs, and expressed as follows [6]:

$$\gamma_k \equiv \frac{V_{\mathrm{QDs}}}{V_{\mathrm{BR}} + V_{\mathrm{QDs}}} \left(\int_{V_{\mathrm{QDs}}} |\psi_k(\mathbf{r})|^2 d^3 r \right)^{-1}, \quad (8)$$

where V_{QDs} is the QD volume, V_{BR} is the volume of the barrier region, and ψ_k is the electron wave function confined in the QD with k as the index of the energy eigenstate. This factor equal to unity for completely delocalized wave functions and smaller than unity for localized wave functions.

To evaluate the value of the EFF for different d_z, we use the wavefunction data in the continuum space obtained by the FEM for the model considering of two QDs, where we implicitly assumed the high density and uniform arrangement of QDs in the x-y plane with the transverse inter-QD spacing $d_x = d_y = 5$ nm, which corresponds to the QD density $\sim 5 \times 10^{11}$ cm^{-2}. The results are given in Tables 1 and 2.

d_z [nm]	1st IB		2nd IB					
1	0.83	0.84	0.73	0.73	0.69	0.71	0.68	0.80
2	0.83	0.85	0.71	0.70	0.71	0.71	0.71	0.8
10	0.82	0.82	0.71	0.67	0.69	0.67	0.67	0.66

Table 1: Relative ratios of the electron probability density inside the QD region. Here, the second IB is less confined in QDs.

d_z [nm]	1st IB		2nd IB					
1	0.45	0.44	0.51	0.51	0.54	0.52	0.55	0.46
2	0.41	0.40	0.47	0.48	0.48	0.48	0.48	0.43
10	0.24	0.24	0.27	0.29	0.28	0.29	0.29	0.30

Table 2: EFF factor values calculated for QDs positioned with the transverse inter-QD spacing $d_x = d_y = 5\mathrm{nm}$

The results indicate that the IB wave functions are strongly confined in the QD region. Moreover, as shown in Table I, the relative ratio of the probability density of an electron inside the QD region is almost independent of the inter-QD spacing. This means that the wave function penetration to the barrier region is almost independent of the inter-QD spacing. Another observation is that the second IB wavefunction is less confined in QDs.

We now consider the detailed balance approach to calculate the efficiency for one electron-hole pair generation per photon [i.e., assumption (ii)] with the help of Planck's formula and the EFF factors, γ_{IB1} and γ_{IB1}, for IB1 and IB2 respectively. For the given structure and considering only IB1, the CB photo current is as follows:

$$\begin{aligned} \frac{I}{q} &= [\dot{N}(E_{13}, \infty, T_{\mathrm{s}}, 0) - \dot{N}(E_{13}, \infty, T_{\mathrm{a}}, \mu_{13})] \\ &\quad + \gamma_{\mathrm{IB1}} [\dot{N}(E_{23}, E_{12}, T_{\mathrm{s}}, 0) - \dot{N}(E_{23}, E_{12}, T_{\mathrm{a}}, \mu_{23})], \end{aligned} \quad (9)$$

where the subscripts 1, 2, and 3 denote the valence, intermediate, and the CB, respectively, and μ_{ij} stands for the quasi-Fermi level (QFL) difference between the ith and the jth bands.

On the other hand, when two IBs (IB1 and IB2) are considered, the CB photo current includes one more element presented by the additional IB (IB2):

$$\begin{aligned} \frac{I}{q} &= \underbrace{[\dot{N}(E_{14}, \infty, T_{\mathrm{s}}, 0) - \dot{N}(E_{14}, \infty, T_{\mathrm{a}}, \mu_{14})]}_{\mathrm{VB-CB}} \\ &\quad + \gamma_{\mathrm{IB1}} \underbrace{[\dot{N}(E_{24}, E_{12}, T_{\mathrm{s}}, 0) - \dot{N}(E_{24}, E_{12}, T_{\mathrm{a}}, \mu_{24})]}_{\mathrm{IB1-CB}} \\ &\quad + \gamma_{\mathrm{IB2}} \underbrace{[\dot{N}(E_{34}, E_{24}, T_{\mathrm{s}}, 0) - \dot{N}(E_{34}, E_{24}, T_{\mathrm{a}}, \mu_{34})]}_{\mathrm{IB2-CB}}, \end{aligned} \quad (10)$$

where the subscripts 1, 2, 3, and 4 denote the valence, lower intermediate, higher intermediate, and the CBs, respectively. This current is delivered at an output voltage that equals to the splitting of the CB and VB Fermi levels, which is given as follows:

$$\mu_{\rm CV} = \begin{cases} \mu_{12} + \mu_{23}, & \text{for one band,} \\ \mu_{12} + \mu_{23} + \mu_{34}, & \text{for two bands.} \end{cases} \quad (11)$$

The chemical potentials are the only remaining neccessary parameters for the calculation of the efficiency. These can be obtained considering by the constraints imposed by Eq. (11) and the continuity equation for each IB assuming ideally separated QFLs for each band. In the case of one IB, the continuity equation can be written as follows:

$$\underbrace{[\dot{N}(E_{12}, E_{13}, T_{\rm s}, 0) - \dot{N}(E_{12}, E_{13}, T_{\rm a}, \mu_{12})]}_{\rm VB-IB} = \underbrace{[\dot{N}(E_{23}, E_{12}, T_{\rm s}, 0) - \dot{N}(E_{23}, E_{12}, T_{\rm a}, \mu_{23})]}_{\rm IB-CB}. \quad (12)$$

In the case of two IBs, there are two continuity equations. The IB1 equation is given by

$$\underbrace{[\dot{N}(E_{12}, E_{13}, T_{\rm s}, 0) - \dot{N}(E_{12}, E_{13}, T_{\rm a}, \mu_{12})]}_{\rm VB-IB1} = \underbrace{[\dot{N}(E_{24}, E_{12}, T_{\rm s}, 0) - \dot{N}(E_{24}, E_{12}, T_{\rm a}, \mu_{24})]}_{\rm IB1-CB}, \quad (13)$$

and the IB2 equation is given by

$$\underbrace{[\dot{N}(E_{13}, E_{14}, T_{\rm s}, 0) - \dot{N}(E_{13}, E_{14}, T_{\rm a}, \mu_{13})]}_{\rm VB-IB2} = \underbrace{[\dot{N}(E_{34}, E_{24}, T_{\rm s}, 0) - \dot{N}(E_{34}, E_{24}, T_{\rm a}, \mu_{34})]}_{\rm IB2-CB}. \quad (14)$$

In the above equations, the IB1–IB2 transition is omitted because its corresponding photon flux is negligible. Finally, by inserting the calculated chemical potentials into Eq. (9) or (10), the delivered power is calculated as $I(\mu_{\rm CV}) \times \mu_{\rm CV}$. Consequently, the efficiency is given by the maximum value of the power divided by the incident solar power per unit area given as $P_{\rm in} = \sigma T^4$, where $\sigma = 5.670 \times 10^{-8}$ [Wm^{-2}K^{-4}] is the Stefan–Boltzmann constant.

To evaluate the performance of QD-IBSCs when $d_z = 10$ nm and $d_x = d_y = 5$ nm (see Fig. 3), we consider how the output power divided by the input power $P_{\rm in}$, defined as $\eta \equiv I \times \mu_{\rm CV}/P_{\rm in}$, depends on $\mu_{\rm CV}$ as shown in Fig. 3.

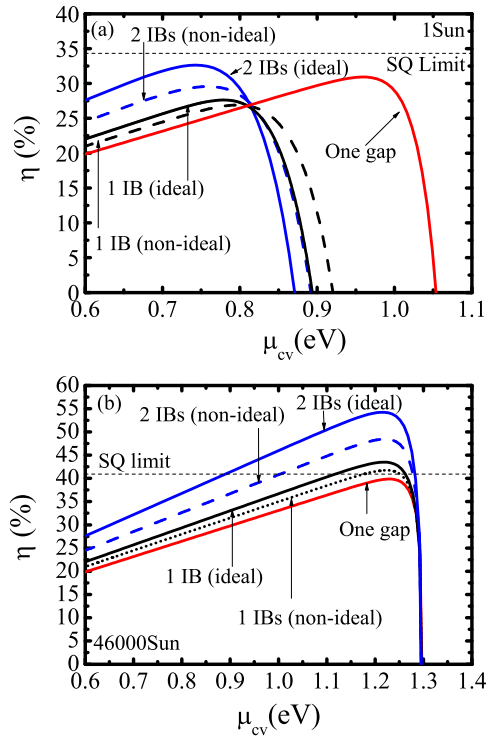

Figure 3: Calculated values of $\eta \equiv I \times \mu_{\rm CV}/P_{\rm in}$ ($\times$100 to see in units of %) vs. $\mu_{\rm cv}$ for both unconcentrated (a) and fully concentrated (b) sunlight are plotted. Non ideal and ideal cases in each figure correspond to the cases with and without considering the IB wave function localization effect through the EFF.

3.2. Numerical results of efficiency

Figures 3(a) and 3(b) show the values of $\eta \equiv I(\mu_{\rm CV}) \times \mu_{\rm CV}/P_{\rm in}$ as a function of $\mu_{\rm CV}$ under one sun and full concentration of solar radiation, respectively, with the results for the ideal case ($\gamma_{\rm IB2} = \gamma_{\rm IB2} = 1$) and the non ideal case with the EFF $\gamma_{\rm IB1} = 0.24$ and $\gamma_{\rm IB2} = 0.286$, are compared (TABLE II and Fig. 3). We also compare an IBSC with only one IB (three levels) and that with two IBs (four levels). As observed in Fig. 3(a), the efficiencies of IBSCs in the case of one-sun solar radiation are lower than the Shockley–Queisser (SQ) limit, even for a solar cell with two IBs, although the use of two IBs increases the efficiency slightly compared with a solar cell with one gap (i.e., without IBs). However, we note that the output voltage $\mu_{\rm CV}/e$ at the maximum power point (at which the efficiency is evaluated) and the open circuit voltage are significantly smaller in the presence of an IB compared with the one-gap solar cell. This is because, in the IB-mediated photo current terms in Eqs. (9) and (10), the recombination current can become more dominant compared with the sun light induced current for the unconcentrated sunlight. This tendency exists even for a solar cell with one IB. However, the smaller QFL difference in an IB mediated process has a stronger impact because of the presence of an IB.

On the other hand, for the case of the full-sun concentration plotted in Fig. 3(b), the output voltage at the maximum power point is almost independent of the number of IBs and the EFF

values. Moreover, the use of two IBs in this case is more effective for enhancing the efficiency than for one-sun illumination. However, the efficiency in the non ideal case is significantly smaller compared with the ideal case, especially when two IBs are considered. This is because the small value of the EFF factors results in a smaller IB-induced current according to Eq. (10). In the case of two IBs, the presence of two IB-related terms in Eq. (10) causes a more significant EFF-induced decrease of the current compared with the case of one IB. Nevertheless, it should be emphasized that even for the non ideal case with a rather localized wave function, it is beneficial to use the IB scheme in improving the efficiency if the sunlight is fully concentrated. Noted that Figs. 3(a) (unconcentrated) and (b) (fully-concentrated) are two limiting cases such that changes in the sunlight concentration will lead to an intermediate behavior.

Before concluding, let us consider some additional effects that we have neglected until now. First, if we further consider ~ 0.2 eV reduction of the output voltage in the presence of the hole-confined levels in the valence-band offset [29], the efficiencies evaluated using the EFF values given in Table 2 are 43% and 42% for one IB and two IBs models, respectively, under the full sunlight concentration. On the other hand, for a single-gap GaAs SC, the maximum efficiency is 38.5%. The higher efficiencies of the IB solar cells demonstrate that the presence of IBs is beneficial even when realistic EFF values are used. Second, if we consider the strain effect, the CB offset, which is the potential barrier height experienced by the CB electron, is reduced by ~ 0.2 eV, as suggested in Ref. [27]. Then, the energy difference between the IB and the CB edge [E_{23} (in the case of one IB) or E_{34} (in the case of two IBs)] assumed thus far must be decreased by this amount. The smaller value of the CB–IB gap essentially gives rise to the increase of the IB mediated photo current and thus the improvement of the efficiency. For instance, the efficiency for one IB solar cell is improved and reaches 35% (56%) for unconcentrated (fully-concentrated) sunlight in an ideal case (i.e, $\gamma = 1$). The efficiency for two IBs is also improved by the strain effect, but the character of the higher IB is more critical because it approaches the CB edge. This means that a careful design of the QD size is important. The qualitative trend of the influence of the IB-electron wave function localization on the QD-IBSC efficiency discussed until now is not changed by the strain-induced shift of the CB-IB gaps.

4. Summary and Conclusion

In this research, we have performed numerical studies of the influence of electron wave function localization on the efficiency limit of QD-IBSC, with a special focus on the roles played by the number of IBs and the sun concentration. As the first step of our analysis, we employed the FEM and TB calculations for cubic QDs as a representative example. The inter-QD separation larger than ~ 5 nm was found to ensure sufficiently thin (< 50 meV) IB band widths.

We then developed an extended version of the detailed balance theory to estimate the efficiency of QD-IBSC with one or two IBs at different sunlight concentrations. The effect of electron wave function confinement in QDs (i.e., thelocalization effect in IBs) was considered using the method of EFF. According to our calculations for the QD structures with the cubic model based on the FEM, the electronic wave functions are strongly localized in the QD region for the realistic inter-QD spacing, resulting in the degradation of the cell efficiency. Nevertheless, the use of IBs was found to be still beneficial for significantly improving the efficiency under full sunlight concentration.

Acknowledgement

This work was supported by JSPS KAKENHI Grant Numbers 25289102, 24656235. The authors would like to thank Enago (www.enago.jp) for the English language review.

References

1) A. Luque and A. Marti, Phys. Rev. Lett. **78**, 5014 (1997).
2) W. Shockley and H. J. Queisser, J. Appl. Phys. **32**, 510 (1961).
3) A. S. Brown and M. A. Green, J. Appl. Phys. **94**, 6150 (2003).
4) P. Wahnon and C. Tablero, Phys. Rev. B **65**, 165115 (2002).
5) K. M. Yu, W. Walukiewicz, J. Wu, W. Shan, J. W. Beeman, M. A. Scarpulla, O. D. Dubon, and P. Becla, Phys. Rev. Lett. **91**, 246403 (2003).
6) A. Marti, L. Cuadra and A. Luque, Physica E, **14**, 150 (2002).
7) A. Luque and A. Marti, Advanced Materials **22**, 160 (2010).
8) A. Marti, E. Antolin, E. Canovas, N. Lopez, A. Luque, C. Stanley, C. Farmer, P. Diaz, C. Christofides, and M. Burhan, Proceedings of the 21st European Photovoltaic Solar Energy Conference, 412 (2006).
9) A. Marti, N. Lopez, E. Antolin, E. Canovas, C. Stanley, C. Farmer, L. Caudra, and A. Luque, Thin Solid Films **511-512**, 638 (2006).
10) Q. Shao and A. A. Bandalin, Appl. Phys. Lett. **91**, 163503, (2007).
11) K. Zaitsu, Y. Kitamura, K. Ono, and S. Tarucha, Appl. Phys. Lett. **92**, 033101 (2008).
12) J. L. Liu, W. G. Wu, A. A. Balandin, G. L. Jin, Y. H. Luo, S. G. Thomas, Y. Lu, and K. L. Wang, Appl. Phys. Lett. **75**, 1745 (1999).
13) S. Kiravittaya, M. Benyoucef, R. Zapf-Gottwick, A. Rastelli, and O. G. Schmidt, Appl. Phys. Lett. **89**, 233102 (2006).
14) J. S. Kim, M. Kawabe, and N. Koguchi, Appl. Phys. Lett. **88**, 072107 (2006).
15) Y. I. Mazur, W. Q. Ma, X. Wang, Z. M. Wang, G. J. Salamo, M. Xiao, T. D. Mishima, and M. B. Johnson, Appl. Phys. Lett. **83**, 987 (2003).
16) Y. Shoji, K. Akimoto and Y. Okada, J. Phys. D: Appl. Phys. **46** (2013).
17) T. Sogabe, Y. Shoji, M. Ohba, K. Yoshida, R. Tamaki, H-F. Hong, C-H. Wu, C-T Kuo, S.Tomic and Y. Okada, Nature, Scientific Reports **4**, Article number: 4792, (2014).
18) A. Luque and A. Marti, Prog. Photovolt. Res. Appl. **9(2)**, 73 (2001).
19) A. Karoui, Appl. Phys. **101**, 236101 (2012).
20) S. Tomic, Phys. Rev. B **82**, 195321 (2010).
21) A. Luque and A. Marti, Advanced Materials, **22**, Issue 2, p 161, January 12, (2010).

22) T. Nozawa, Y. Arakawa, Appl. Phys. Lett. **98**, 171108 (2011).
23) T. Nozawa, Y. Arakawa, J. Appl. Phys. **113**, 243102 (2013).
24) A. Luque, P. G. Linares, E. Antolin, E. Canovas, C. D. Farmer, C. R. Stanleyand A. Marti, Appl. Phys. Lett. **96**, 013501 (2010).
25) A. Marti, E. Antolin, E. Canovas, N. Lopez, P. G. Linares, A. Luque, C. R. Stanley, C. D. Farmer, Thin Solid Films **516**, 30 (2008).
26) Y. C. Ruan and W. Y. Ching, J. Appl. Phys. **62**, 2885 (1987).
27) O. L. Lazarenkova and A. A. Balandin, J. Appl. Phys. **89**, 5509 (2001).
28) S.-S. Li, J.-B. Xia, Z. L. Yuan, Z. Y. Xu, W. Ge, X. R. Wang, Y. Wang, J. Wang, and L. L. Chang, Phys. Rev. B**54**, 11575 (1996).
29) P. G. Linares, C. D. Farmer, E. Antolin, S. Chakrabarti, A. M. Sanchez, T. Ben, S. I. Molina, C. R. Stanley, A. Marti, A. Luque, Energy Procedia **2**, 133 (2010).